Parametric Interaction of VLF and ELF Waves in the Ionosphere and Impact on Energetic Electrons in a Radiation Belt

V. Sotnikov, J. Caplinger, T. Kim
Air Force Research Laboratory, Wright-Patterson AFB, OH 45433, USA

E. Mishin
Air Force Research Laboratory, Kirtland AFB, NM 87117, USA

N. Gershenzon and A. Sharma
Wright State University, Fairborn, OH 45324, USA

D. Main
Tech-X Inc., Boulder, CO 80303, USA

Abstract

Generation of Very Low Frequency (VLF) electromagnetic whistler wave due to the parametric interaction of quasi-electrostatic VLF waves known as lower Oblique Resonance (LOR) waves and Extremely Low Frequency (ELF) waves as well as Ion Acoustic (IA) will be analyzed. Two possible scenarios will be analyzed. In the first scenario quasi-electrostatic LOR waves and ELF waves necessary for parametric generation of electromagnetic whistler waves are excited by conventional loop and dipole antennas. In the second case they are naturally excited by fluxes of energetic particles in the plasmospheric boundary layer.

Whistler waves interact with Radiation Belt (RB) electrons via cyclotron resonance. This interaction leads to enhanced pitch angle diffusion and shifting energetic electrons towards the loss cone. In order for this interaction to be efficient it is necessary to create certain level of finite amplitude VLF electromagnetic whistler waves in the interaction region. In the case of conventional antenna sources as well as for naturally excited VLF waves, a great deal of the source power is radiated not as a whistler wave but as a quasi-electrostatic Low Oblique Resonance (LOR) mode which does not propagate on great distances from the source region. We present new results on parametric interaction of LOR waves with ELF and IA waves to demonstrate the possibility to overcome this difficulty. It will be shown that interaction of LOR waves with very low frequency waves gives rise to electromagnetic whistler waves on combination frequencies.

1. Introduction

The generation of very low frequency (VLF) waves by antennas in plasma is an important topic because of the wide use of antennas in space and laboratory applications, both military and civilian. There have been a considerable amount of publications related to the excitation of VLF waves by a loop antenna. Between 1969 and 1974 Wang and Bell published a series of papers detailing the theory of power radiated from electric dipole and loop antennas in plasmas [Wang and Bell, 1969, 1970; 1972a; 1972b; Wang, 1974; Bell and Wang, 1971]. Three of these articles [Bell and Wang, 1971; Wang and Bell, 1972b; Wang, 1974] concerned loop antennas, with the two [Wang and Bell, 1972a; Wang, 1974] taking into consideration arbitrary angles of antenna orientation and warm plasma effects, respectively. Calculation of power radiated by a loop antenna, based on use of magnetization created by a loop was carried out by Chugunov [1973]. Different approach to analysis of electromagnetic fields excited by a loop antenna based on use of a Green function was implemented by Karpman [1987]. In the paper by Sotnikov et al [1993], the procedure to obtain resonance surfaces in the vicinity of a loop antenna with the loop plane containing an external magnetic field with no azimuthal symmetry in the system, was developed. In the same paper, the expression for calculating radiated power based on the approach developed by Chugunov [1973] was obtained for an arbitrary angle between the loop plane and direction of an external magnetic field. However, in all cited above papers uniform current along a loop antenna was suggested. This issue was addressed in the paper by Kondrat'ev and Kudrin [1992], where it was shown that inhomogeneity in the distribution of the electric current in the loop can lead to increase in the portion of radiated power going into quasi-electrostatic part of the wave spectrum. However, for ring magnetic currents effect of the current inhomogeneity is less pronounced. In the paper by Kudrin et al [2001], the current distribution and the input impedance of a circular thin strip-loop antenna is analyzed and results are applied for the analysis of antenna characteristics in a plasma with ionospheric parameters.

It is known that when a loop radius is small in comparison with the wavelength of an excited wave, the portion of the radiation field that goes directly into the electromagnetic spectrum of a VLF wave - the whistler mode, is small (less than 3%) in comparison with the wave energy going into the quasi-electrostatic whistler wave component - low oblique resonance (LOR) mode. For this reason, the efficiency of VLF antennas for generation of electromagnetic waves, which can propagate large distance

from the source region, is very limited. For many ionosphere applications it is important to increase the level of the radiated power exciting the electromagnetic part of the wave spectrum—whistler waves.

The efficiency of antenna may be increase by parametric mechanism of transformation of quasi-electrostatic whistler waves excited by a loop antenna operating at frequency ω on density perturbations produced by a dipole antenna (low frequency source) with frequency Ω which excites ionacoustic waves with frequency above the ion cyclotron frequency but well below the lower hybrid frequency [Sotnikov et al, 2018]. In this case, whistlers will be excited on combination frequencies $\omega \pm \Omega$. The dipole is placed in the center of the loop and lies in its plane. Such an arrangement may be regarded as a parametric antenna for enhanced excitation of whistlers. It has been pointed out that in the ionosphere ion-acoustic waves are strongly dampened because electron and ion temperatures are approximately equal. Even in this case, due to the presence of an external source, it is possible so-called ion-acoustic quasi-modes can exist, which create desired density perturbations in the vicinity of an antenna. In reality, in the ionosphere with presence of a powerful VLF antenna, the temperature of electrons can substantially exceed ion temperature. This enhancement was observed at distances up to two kilometers from the VLF source during the CHARGE 2B experiment [Sotnikov et al, 1995]. We first consider the linear theory of antenna radiation in ionosphere plasma. Examples of computer simulations will be presented. Then we will describe the basics of nonlinear theory (parametric interaction).

In the second part of the paper we present the results of numerical simulations of nonlinear coupling between quasi-electrostatic lower hybrid oblique resonance (LOR) and fast magnetosonic (MS) waves, which was suggested to explain the observations of VLF electromagnetic emissions at frequencies well above the lower hybrid resonance frequency in the Turbulent Plasmasphere Boundary Layer (TPBL). These emissions represent a distinctive subset of the substorm/storm-related VLF whistler activity contributing to the alteration of the outer radiation belt boundary. As the TPBL is interior to the plasma sheet inner boundary and thus devoid of substorm-injected keV electrons, the "standard" whistler generation mechanism must be excluded. Numerical solution of derived equations show that the parametric coupling of LOR and ELF waves creates VLF electromagnetic emissions with the spectral characteristics consistent with the observations.

2. VLF Waves in the Ionosphere

We analyze excitation of waves with frequencies ω several times above the lower hybrid resonance frequency, but below the one half of electron cyclotron frequency *i.e.:*

$$\omega_{LH} < \omega < \frac{1}{2}\omega_{ce} \ , \tag{1}$$

where the lower hybrid frequency ω_{LH} in the case when $\omega_{ce}^2 = \omega_{pe}^2$ is given by:

$$\omega_{LH}^2 = \frac{\omega_{pi}^2}{1+\omega_{pe}^2/\omega_{ce}^2}. \tag{2}$$

Here ω_{LH} is the lower hybrid resonance frequency, ω_{ce} is an electron cyclotron frequency and ω_{pe} is an electron plasma frequency. Under these conditions, only one mode is excited in a cold plasma and the main features of the radiation far away from the source can be understood from the plot analogous of wave refractive index surface. This plot can be obtained using the expression for the dispersion of VLF waves:

$$\omega^2 = \frac{\omega_{LH}^2}{[1+\omega_{pe}^2/(k^2c^2)]^2}\frac{m_i}{m}\frac{k_z^2}{k^2}, \tag{3}$$

where $k^2 = k_\perp^2 + k_z^2$, k_z is the wave vector component along the magnetic field and $k_\perp$ is the perpendicular component. Figure 1 schematically plotting the wave vector component k_z against $k_\perp$ for a given ω.

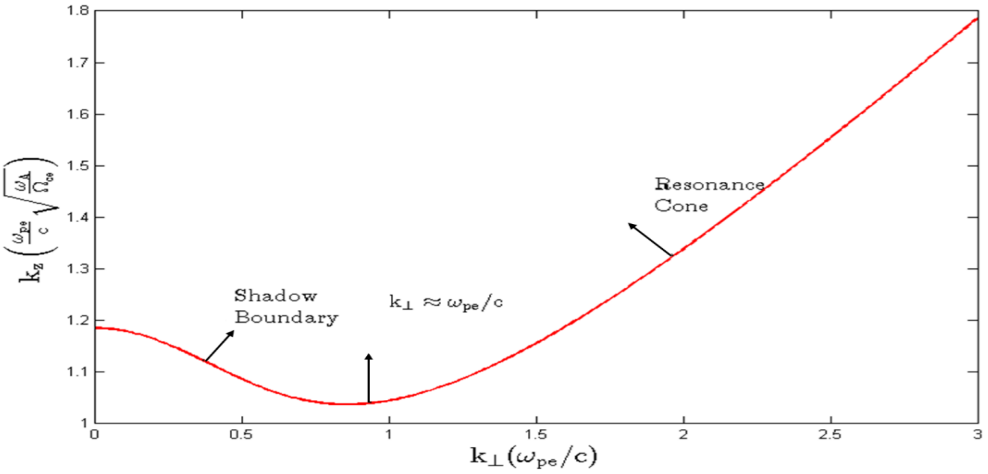

Figure 1: Wave number surface for a constant $\omega_{LH} < \omega = \omega_{ce}$ with three critical points.

A great deal of the source power is radiated as quasi-electrostatic whistler waves with $\omega_{pe}^2/(k^2c^2) = 1$. The real electromagnetic mode, the whistler wave, with $\omega_{pe}^2/(k^2c^2) ? 1$is radiated in oblique directions up to an angle ~ 19.5°, which is the shadow boundary determined by the long wavelength inflexion point and these waves radiate weakly compared to other portion of the spectrum. It can be shown [Fisher and Gould, 1971], that radiation goes out in the direction of the normal to the $k_z(k_\perp)$ curve and decreases with the distance R as R^{-1} everywhere with the exception of the three critical points determining three critical directions: the two inflexion points $d^2k_z/dk_\perp^2$ where the field decreases as $R^{-5/6}$. The first inflection point corresponds to the critical angle 19.5°. The third critical point corresponds to minimum $d^2k_z/dk_\perp^2 = 0$, where the field decreases as $R^{-1/2}$, which gives the radiation along the external magnetic field.

3. Excitation of VLF Waves by a Loop Antenna

Here we will discuss the distribution of an electric field excited by a loop antenna and we will calculate total radiated power and power radiated into the electromagnetic part of the VLF wave spectrum – whistler waves. This is important especially for active experiments in the ionosphere since whistler waves can propagate a great distance from the source region.

Logarithmic type singularities along the resonance cones are displayed when the plane of a loop is perpendicular to an external magnetic field [Fisher and Gould, 1971; Karpman, 1986]. This is schematically represented in Figure 2.

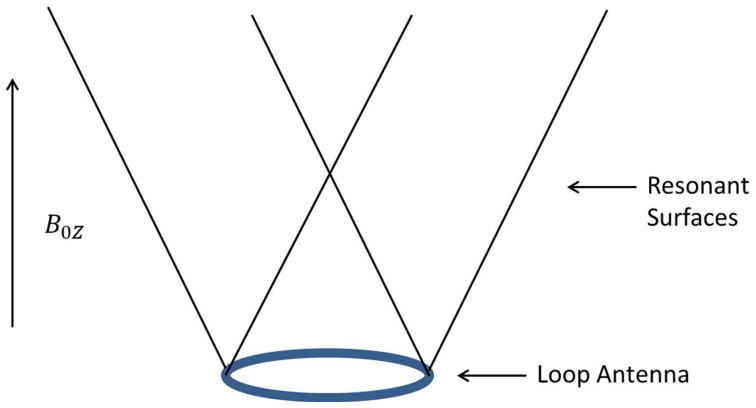

Figure 2. Resonant surfaces of a loop antenna. On these surfaces, the wave potential experiences logarithmic type singularity

In another case, when magnetic field lies in a loop plane (see Figure 3) there are two resonance surfaces, one inside the other. The method of obtaining these surfaces was suggested by Sotnikov et al. [1993].

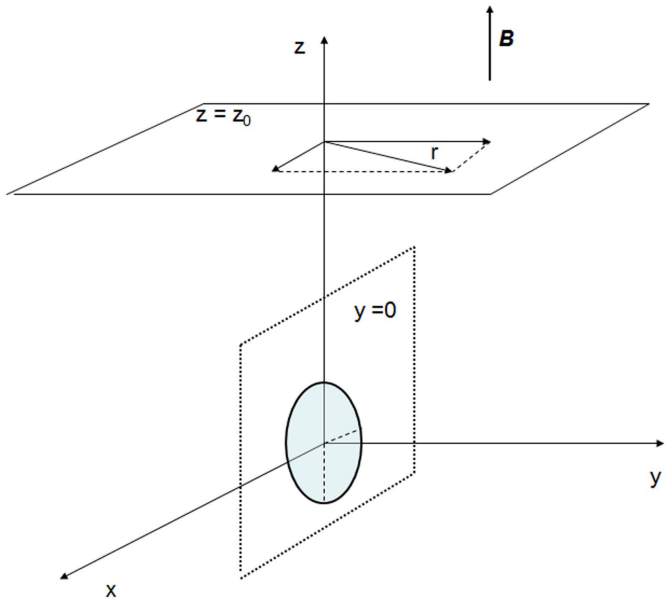

Figure 3: The coordinate system used. The loop antenna is in the $y = 0$ plane and an external magnetic field is along the z axis.

The potential of the electric field generated by a loop antenna is:

$$\Phi_0 = \frac{g\omega M_z}{c(1+\gamma^2)}\left[\frac{1}{R} + \frac{1}{\gamma(\gamma^2 \mathrm{z}^2 - \mathrm{r}^2)^{1/2}}\right] + \frac{\omega}{c}\frac{z}{r^2}\left[\mathrm{i}(\mathbf{M}\times\mathbf{r})_z - \frac{g}{\eta(1+\gamma^2)}(\mathbf{M}\cdot\mathbf{r})\right]\left[\frac{1}{R} - \frac{\gamma}{(\gamma^2 \mathrm{z}^2 - \mathrm{r}^2)^{1/2}}\right], \quad (4)$$

where $\boldsymbol{M}$ is a magnetic moment, ω is frequency of oscillation, $R^2 = x^2 + y^2 + z^2$, $r^2 = x^2 + y^2$,

$$\varepsilon_{xx} = \varepsilon_{yy} = \varepsilon, \varepsilon_{xy} = -\varepsilon_{yx} = -ig, \varepsilon_{zz} = \eta, \varepsilon = 1 + \sum_\alpha \frac{\omega_{p\alpha}^2}{\omega_{c\alpha}^2 - \omega^2}, g = \sum_\alpha \frac{\omega_{p\alpha}^2 \omega_{c\alpha}}{\omega(\omega_{c\alpha}^2 - \omega^2)} \frac{e_\alpha}{|e_\alpha|}, \eta = 1 - \sum_\alpha \frac{\omega_{p\alpha}^2}{\omega^2} \alpha = e, i,$$

$\gamma^2 = -\varepsilon/\eta$, If $r > \gamma|z|$ then $(\gamma^2 \mathrm{z}^2 - \mathrm{r}^2)^{1/2} = +i(\mathrm{r}^2 - \gamma^2 \mathrm{z}^2)^{1/2}$.

The electric field becomes infinite (has a logarithmic singularity) on so-called resonance conical surfaces. These surfaces have a complicated shape and could be described by the following parametric relations:

$$X_s = \gamma^2(\mathrm{Z}_s + a\cos\Theta_s)\tan\Theta_s + a\sin\Theta_s,$$

$$Y_s^2 = \gamma^2(\mathrm{Z}_s + a\cos\Theta_s)^2(1-\gamma^2 a\tan^2\Theta_s),$$

where $X_s, \mathrm{Y}_s, \mathrm{Z}_s$ are point coordinate on the surface and parameter Θ_s varies with limits $\alpha < \Theta_s < \alpha$ and $\pi - \alpha < \Theta_s < \pi + \alpha$, where $\alpha = \arctan(1/\gamma)$. Figure 4 shows internal and external resonance surfaces (asymptotic cones) in close proximity to the antenna. On these surfaces excited field experiences logarithmic type singularities.

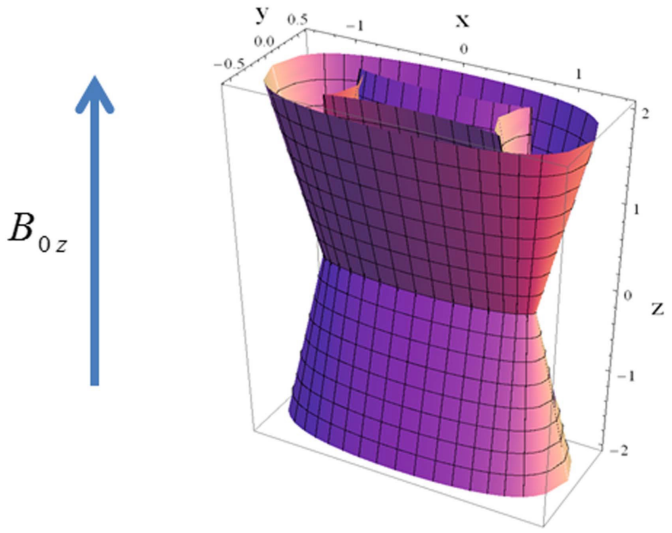

Figure 4: Example of two resonance surfaces (internal and external) of a loop antenna with an external magnetic field in a loop plane.

The asymptotes of the field close to the resonance surfaces are:

$$E_x\ ;\ \frac{i\omega a I_A \gamma}{\sqrt{2}c^2}\frac{\tan\Theta_s \sin\Theta_s}{\sqrt{f_\theta'''}}\ln\left|\frac{2\Delta f}{f_\theta'''}\right| = E_{x0}\ln\left|\frac{2\Delta f}{f_\theta'''}\right|$$

$$E_y\ ;\ \frac{i\omega a I_A}{\gamma\sqrt{2}c^2}\frac{\mathrm{Y}_s \sin\Theta_s}{(\mathrm{Z}_s + a\cos\Theta_s)\sqrt{f_\theta'''}}\ln\left|\frac{2\Delta f}{f_\theta''}\right| = E_{y0}\ln\left|\frac{2\Delta f}{f_\theta''}\right|, \qquad (5)$$

$$E_z\ ;\ \frac{i\omega a\gamma I_A}{\sqrt{2}c^2}\frac{\sin\Theta_s}{\sqrt{f_\theta'''}}\ln\left|\frac{2\Delta f}{f_\theta''}\right| = E_{z0}\ln\left|\frac{2\Delta f}{f_\theta''}\right|,$$

where $f_\theta''' = -2a\frac{\gamma^2 Z_s}{\cos\Theta_s} - 2a^2(1+\gamma^2)\cos^2\Theta_s$

and $\Delta f = 2a\gamma^2(Z_s + a\cos\Theta_s)(z - Z_s) - 2(X_s - a\sin\Theta_s)(x - X_s) - 2Y_s(y - Y_s)$.

Figure 5 shows spatial distribution of absolute value of electric field generated by a loop antenna. For the realistic ionosphere conditions, the electric field in close proximity to the cones is in the order of 10-100 V/m, which is the same order of magnitude as was estimated by Sotnikov et al. [1993].

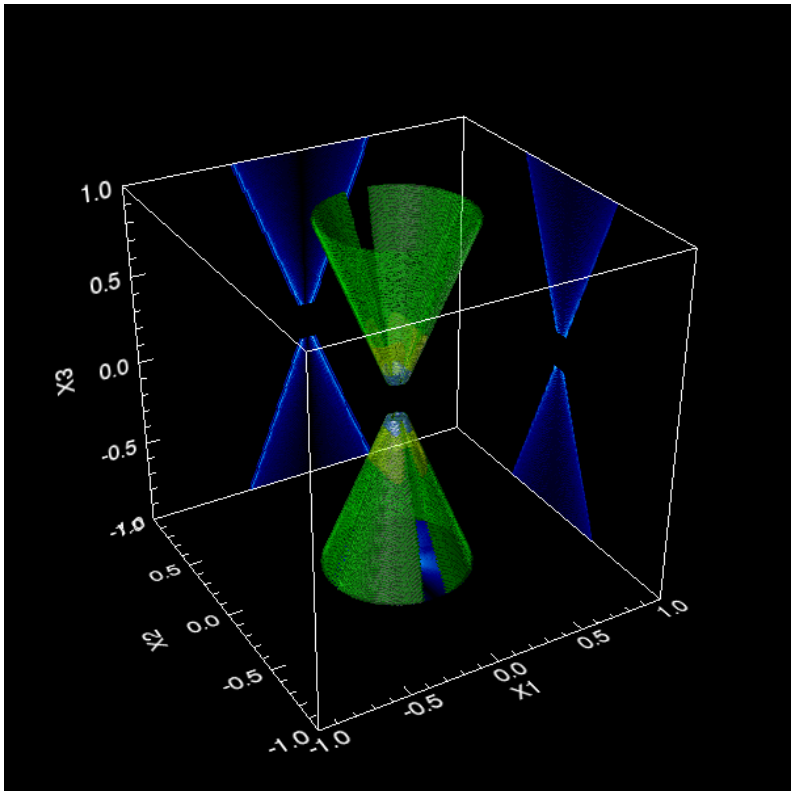

Figure 5. 3D spatial distribution of absolute value of electric field generated by a ring VLF antenna.

To calculate the total radiated power and power which goes to the electromagnetic part of the VLF wave spectrum for whistler waves, we consider a time harmonic loop current source, $I_0 exp[j\omega t]$, and begin with the expression for the radiated power [Sotnikov et al, 1993]:

$$P = P_1 + P_2\ , \qquad (6)$$

$$P_1 = \frac{\pi}{2} I_A^2 \frac{a\omega}{c^2} F_1\ , \qquad P_2 = \pi I_A^2 \frac{a\omega}{c^2}\frac{a^2\omega_{pe}^2}{c^2}\frac{\omega^4}{\omega_{ce}^4} F_2 \sin^2(\alpha)\ ,$$

where α is the angle between normal to loop antenna plane and main magnetic field direction,

$$F_1 = \int_0^{2\pi} d\varphi \int_0^{\infty} dk \frac{k}{k_{res}} J_1^2(\sqrt{\rho})[1 - \frac{k^2(1+\omega^2/\omega_{ce}^2)}{B}] ,$$

$$F_2 = \int_0^{2\pi} d\varphi \cos^2(\varphi) \int_0^{\infty} dk \frac{k^3}{k_{res}} \frac{J_1^2(\sqrt{\rho})}{B\rho},$$

$$k_{res}^2 = \frac{\omega^2 a^2 \omega_{pe}^2}{\omega_{ce}^2 c^2} - \frac{1}{2}(1 - \frac{\omega^2}{\omega_{ce}^2}) + \frac{1}{2} B ,$$

$$B = \sqrt{(1+\frac{\omega^2}{\omega_{ce}^2})^2 k^4 + 4\frac{\omega^2}{\omega_{ce}^2}\frac{a^2\omega_{pe}^2}{c^2} + 4\frac{\omega^2}{\omega_{ce}^2}\frac{a^4\omega_{pe}^4}{c^4}} ,$$

$\rho = k^2 \cos^2(\varphi) + (\mathrm{k}_{res}\sin(\alpha) - k\sin(\varphi)\cos(\alpha))^2$. Here k is normalized by a (radius of loop antenna).

Results of calculation are depicted in Fig. 6. Figure 6(a) shows the total radiated power as a function of the angle between the antenna normal and the magnetic field. Figure 6(b) shows the long wavelength radiated power found by integrating in $k_\perp$ out to $\delta = k_\perp c/\omega_{pe} = 0.1$.

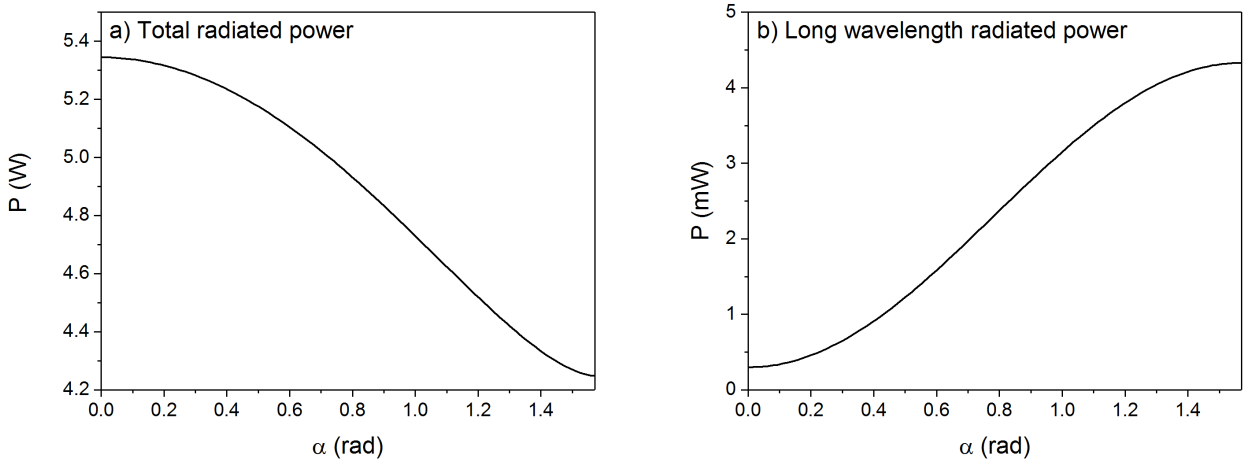

Figure 6: (a) Total radiated power versus angle between the antenna loop normal and the magnetic field. (b) Radiated power for long wavelengths within the Story angle (δ≤0.04) versus angle between the antenna normal and the magnetic field. Plasma parameters correspond to ionosphere conditions: electron density $n_e = 3\times10^4 cm^{-3}$, magnetic induction $B_0 = 0.3G$. The loop antenna had a current of $I_0 = 100\,A$, frequency $\omega = 6\times10^4 s^{-1}$, and a radius of $R = 10\,m$.

4. Parametric Excitation of VLF Waves

Nearly monochromatic signals injected from ground-based VLF transmitters are known to experience bandwidth expansion as they traverse the ionosphere and magnetosphere [Bell et al., 1983; Titova et al. 1984; Inan and Bell, 1985; Tanaka et al, 1987; Chmyrev et al, 1989] and magnetosphere [Bell and Ngo, 1988]. Several mechanisms have been proposed to explain this phenomenon based upon linear and nonlinear scattering assuming existence of magnetic-field-aligned plasma density irregularities. In the absence of ionosphere irregularities a mechanism based on a parametric instability was proposed by Riggin and Kelly [1982], Lee and Kuo [1984] and Groves et al, [1988].

Reports on sideband signals associated with VLF transmitter signals are rather scarce. Spectral peaks have been identified near the magnetic equatorial plane on the ISEE satellite at approximately ± 55 Hz of the carrier frequency (13.1 and 13.6 kHz) of Omega pulses [Bell, 1985]. Similar peaks seem to be observed on the COSMOS 1809 satellite and generated in the ionosphere by the carrier frequency 19 kHz [Chmyrev et al, 1989]. Sidebands at approximately ± 500 Hz of the carrier frequency (11.9 and 12.65 kHz) of Alpha pulses have been observed in the ionosphere by the AUREOL 3 satellite [Tanaka et al, 1987; Lagoutte et al, 1989].

At first sight, the 50-Hz sidebands observed on AUREOL 3 seem to correspond the Riggin and Kelly [1982] prediction in which the transmitted wave decays into a lower hybrid wave and an ion-acoustic type of oscillation. To account for the existence of two symmetric spectral peaks, one may replace the three-wave parametric instability considered by these authors by a four-wave parametric instability (or modulational instability) as suggested by Groves et al [1988]. According to this scheme, the ELF branch is due to a purely growing electrostatic mode with wave vector $\boldsymbol{k}$ large enough to provide sidebands $\pm|kV_s|$ off the transmitter frequency (V_s is the satellite velocity). This mode is excited in course of a four-wave process by the incident VLF transmitter wave. In our case, the ELF wave branch is clearly electromagnetic and as such is of natural origin. Therefore, another explanation in accord with this experimental data has to be found.

Sotnikov et al [1991] proposed another mechanism for the production of 500-Hz sidebands. It is based on nonlinear coupling between the transmitted wave and the ELF emission above the local proton gyrofrequency. The sidebands are shown to be forced oscillations, excited only where the coupling take place.

We consider the nonlinear coupling model described in the articles [Falla et al, 1987; Sotnikov et al, 1991; 1994]. The equation for analysis of nonlinear interaction of VLF waves with ion-acoustic (IA) waves in magnetized plasma was derived in [Sagdeev et al, 1977]. Electric and magnetic fields in a

magneto-sonic type VLF wave were represented through a scalar potential φ and a vector potential $\mathbf{A}$ with the Coulomb gauge, $\mathbf{E}=-\nabla\varphi-\frac{1}{c}\frac{\partial\mathbf{A}}{\partial t}$ and $\mathbf{B}=\nabla\times\mathbf{A}$ with $\nabla\cdot\mathbf{B}=0$. For analysis of parametric excitation of electromagnetic whistler waves due to transformation of LOR waves with frequency ω excited by a loop antenna, on IA oscillations excited by another low frequency source with frequency Ω ($\omega_{ci}\ll\Omega\ll\omega$) we can modify the equation derived in [Sagdeev et al, 1977]. Whistlers are excited on combination frequencies $\omega_{\text{I}}=\omega\pm\Omega$, and we are interested in the excitation of whistlers on frequencies from the range $\omega_{\pm}\sim(2\div10)\omega_{LH}$. For the parametrically excited whistler wave's Fourier component potential $\varphi_{k\_}$ with $\omega\_=\omega-\Omega$ and $k\_=k-k_s$ we can write:

$$\frac{\partial^2}{\partial t^2}\varphi_{NL}^t+\omega_{ce}^2\frac{c^4}{\omega_{pe}^2}\Delta\frac{\partial^2}{\partial k_z^2}\varphi_{NL}^t=-\frac{1}{n_0}\omega_{ce}\frac{c^2}{\omega_{pe}^2}\frac{\partial}{\partial t}\left[\nabla\delta n_{s,}^*\nabla\varphi^l\right]_z \tag{7}$$

In equation (1) φ_{NL}^t is the potential associated with a parametrically excited whistler mode, φ^l is the potential of LOR mode excited by a loop antenna and δn_s is ion-acoustic type density perturbation excited by a dipole antenna. Equation (1) can be used to analyze the generation of whistlers due to parametric interaction of LOR waves with low frequency ion-acoustic type density perturbations excited by a dipole antenna. Using previously obtained expressions for φ^l and δn_s for the case when an external magnetic field is perpendicular to the loop plane, we arrive to the following expression for components of the electric field in the plane perpendicular to an external magnetic field:

$$E_{x,NL}^t=-\frac{1}{12\sqrt{2}}\frac{1}{en_0}\frac{\omega\_\omega\omega_{pe}^2\Omega^2}{\omega_{ce}c^4v_s^3}R_a^2d_0J_aJ_d\frac{\sin\Phi}{r}\left(i\sin\Phi-\frac{z}{r}\cos\Phi\right) \tag{8}$$

$$E_{y,NL}^t=-\frac{1}{12\sqrt{2}}\frac{1}{en_0}\frac{\omega\_\omega\omega_{pe}^2\Omega^2}{\omega_{ce}c^4v_s^3}R_a^2d_0J_aJ_d\frac{\sin\Phi}{r}\left(-i\cos\Phi-\frac{z}{r}\sin\Phi\right) \tag{9}$$

Knowledge of parametrically excited electric fields in a whistler mode allows us to proceed with the calculation of power radiated by parametrically excited nonlinear current $\mathbf{J}_{NL}(\mathbf{r},\mathbf{t})$:

$$\mathbf{J}_{NL}(\mathbf{r},\mathbf{t})=-e\delta n_s\mathbf{v}_{LOR}, \tag{10}$$

here δn_s is the ion-acoustic type density perturbation excited by a low frequency dipole and $\mathbf{v}_{LCR}$ is the speed of electrons in the presence of LOR wave excited by a loop antenna. To find δn_s we can use equation for excitation of ion-acoustic waves by a dipole antenna. In the simplest case of a point dipole antenna with the current density in the dipole given by $\delta\mathbf{j}_c=J_dd_0\delta(\mathbf{r})\mathbf{e}_x$ we have:

$$\delta n_s(x,y,z,t)=\frac{J_ad_0\Omega}{4\pi eV_s^2}\frac{x}{R^3}\left(i-\frac{\Omega R}{V_s}\right)exp\{i[\Omega(t-R/V_s)]\}, \tag{11}$$

where $R = [x^2 + y^2 + z^2]^{1/2}$. To find velocity $\mathbf{v}_{LCR}$ which appears due to the presence of an electric LOR wave field excited by a loop antenna we can use the electron equation of motion in a drift approximation. Resulting expressions for $\mathbf{v}_{LCR}$ are:

$$\mathbf{v}_{LOR} = c\frac{\mathbf{E}_{LOR}\times\mathbf{B}_0}{B_0^2}, \quad (12)$$

where $\mathbf{E}_{LOR}$ is the field of quasielectrostatic LOR waves excited by a loop antenna. Now the expression for the radiated power of parametrically excited whistler waves can be written as:

$$P_{NL} = -\frac{1}{2}Re\int \mathbf{j}_{NL}^{*}\cdot\mathbf{E}_{NL}d^3r \quad (13)$$

Using the same set of plasma parameters from equation (13) one can obtain the value of power radiated into an electromagnetic part of VLF wave spectrum – whistler waves. Taking the current in a low frequency dipole antenna $J_d = 4\ A$, the value of radiated power when the loop plane is perpendicular to an external magnetic field is $P_{NL} = 0.11$ Watts. The value of radiated power (at the angle $\alpha = 0$) of a single loop antenna can be found to be $P_L = 0.1$ Watts. Increasing the current in a dipole antenna to $J_d = 10\ A$ for parametrically excited radiated power we have $P_{NL} = 0.65$ Watts. These examples show that parametric mechanism of excitation is very effective and produces much higher radiated power output in electromagnetic part of the VLF wave spectrum.

Further development of the problem of parametrically generated plasma turbulence has been developed in the articles by Sotnikov et al, [1991; 1994] as attempt to explain appearance of symmetric sidebands emissions (secondary peaks in wave power) observed in multiple ionosphere-magnetosphere experiments, e.g. Figures 7 and 8. In these articles, the nonlinear coupling of the VLF transmitter signal to natural ELF emission is invoked to explain the sidebands. It was shown that the nonlinear current excited by the beats of VLF and ELF waves is strong enough to produce observed amplitude of sideband emissions.

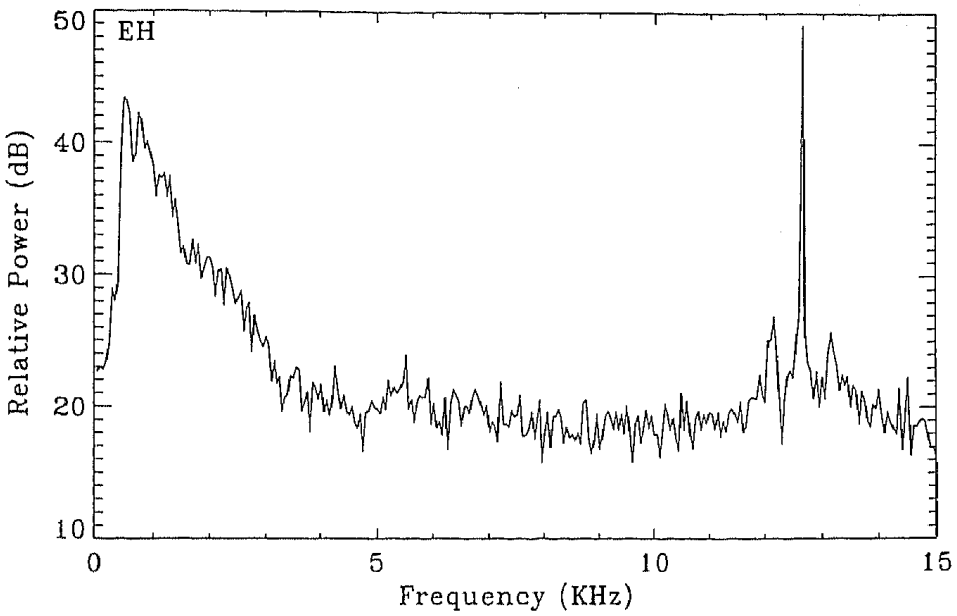

Figure 7. Averaged power spectral density of electric field. ELF natural emission at 500 Hz, VLF transmitted emission at 12.65 kHz, sidebands at frequencies (12.65 + 0.5) kHz and (12.65 - 0.5) kHz. This data were observed in ionosphere on AUREOL 3 satellite during experiments in framework of ARCAD project [Tanaka et al 1987]

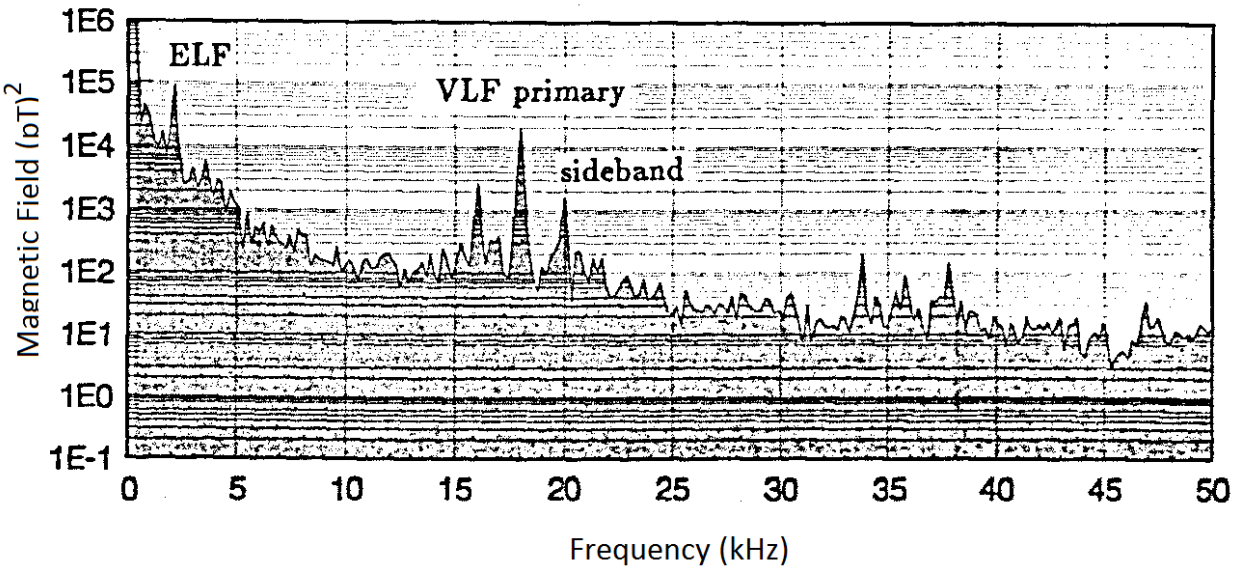

Figure 8. ELF natural emission at 2 kHz, VLF transmitted emission at 17.95 kHz, sidebands at frequencies (17.95 + 2) kHz and (17.95 - 2) kHz. This data were observed during Cooperative High-Altitude Rocket Gun Experiment (CARGE 2B) carried out in March 1992.

The nonlinear coupling of the VLF and ELF modes can cause a beat-wave field at the combination frequency given by

$$\omega_{\pm} = \omega_{k_1} \pm \omega_{k_2}, \tag{14}$$

which can result in sideband emissions. The sideband wave numbers are matched according to

$$k_{\pm} = k_1 \pm k_2 \tag{15}$$

Note that sidebands are not plasma eigenmodes but forced oscillations excited only where VLF to ELF wave coupling take place.

Using the cold plasma approximation the equations for the perpendicular to magnetic field sideband electric field components can be derived in the form [Sotnikov et al 1994]:

$$\begin{aligned} E_{\perp k_+} &= \frac{e}{2m}\frac{k_+}{\Omega_e \delta\omega_+}[E_{k_1} \times E_{k_2}]_z \\ E_{\perp k_-} &= \frac{e}{2m}\frac{k_-}{\Omega_e \delta\omega_-}[E_{k_1} \times E_{k_2}]_z \end{aligned}, \tag{16}$$

where

$$\frac{\delta\omega_{\pm}}{\Omega_e} = \frac{k_{z1}/k_1}{1+\omega_{pe}^2/(k_1^2c^2)} \pm \frac{k_{z2}/k_2}{1+\omega_{pe}^2/(k_2^2c^2)} - \frac{(k_{z1} \pm k_{z2})/k_{3\pm}}{1+\omega_{pe}^2/(k_{3\pm}^2c^2)}, \tag{17}$$

$k_{3\pm}^2 = k_1^2 + k_2^2 \pm 2k_1k_2\cos(\theta)$ and θ is the angle between the wavevectors.

Sidebands may be a result of nonlinear coupling of the VLF transmitter wave and the natural ELF emission above the local proton gyrofrequency. The VLF wave propagate through the ionosphere as a whistler mode.

$$\omega_{k_1} = \Omega_e \frac{k_{1z}/k_1}{1+\omega_{pe}^2/(k_1^2c^2)} \tag{18}$$

For the transmitted frequency $\omega/2\pi = 12\,kHz$, the corresponding wave number is $k_1 \approx 2\cdot10^{-4}\,cm^{-1}$. For the known parameters whistler propagates with $\omega_{pe}^2/(k_1^2c^2) \approx 1$ at large angle to the magnetic field.

The characteristic frequency ω_{k_2} of the ELF wave is slightly above the ion gyrofrequency and $k_2 \approx 3\cdot10^{-5}\,cm^{-1}$. These waves generally propagate at large angle to the geomagnetic field. As $\omega_{pe}^2/(k_2^2c^2) >> 1$, it is described by

$$\omega_{k_2} = \Omega_e \frac{k_{2z}}{k_2}\frac{k_1^2c^2}{\omega_{pe}^2}, \tag{19}$$

Ω_e is the electron cyclotron frequency.

5. Excitation of Whistler Waves by a Parametric Antenna: LSP Simulation

A well-developed particle-in-cell plasma simulation code called Large Scale Plasma (LSP) [Welch et al, 2006] was used to perform 3D simulations of VLF field excitation by a conventional loop antenna and by a parametric antenna. We present 3D simulation results on generation of electromagnetic and quasi-electrostatic VLF waves by a loop antenna and by a parametric antenna, which combines both a VLF loop and an ELF dipole antenna. In order to resolve the long wavelength portion of the whistler waves (the portion which is largely electromagnetic), it was necessary to take a large spatial grid ($\Delta x = \Delta y = \Delta z = 200\, cm$), in order to expand the total simulation volume. This however, made it impossible to resolve short wavelength ion-acoustic (IA) waves. Thus in 3D the authors were unable to generate both VLF and IA waves simultaneously because it was overly computationally expensive even using a highly parallelized HPC. However, fast magnetosonic or ELF waves, which can be excited at the same frequency as the IA waves, are resolvable alongside the VLF waves. For this reason, the simulations are restricted to the cases of a single VLF loop antenna and a parametric antenna consisting of a VLF loop and an ELF dipole antenna.

In the case of 3D simulations a square loop antenna is used to excite whistler waves. This antenna is placed in the center of the simulation domain, with its plane perpendicular to the z-axis, with an effective radius of 6 meters. A 12 meter linear dipole occupies the same plane in the case of the parametric antenna. The applied background magnetic field of 0.3 Gauss is directed along the z-axis. For the boundaries, perfectly-matched layers (PML) were used in order to minimize reflections. The initial plasma density was $10^5 cm^{-3}$. The loop antenna in both the single loop case and the parametric antenna case was excited with a 100 A current oscillating with the frequency $\omega = 1.31\times10^6\ \mathrm{rad/s}$. For chosen plasma and magnetic field parameters this frequency is ten times larger than lower hybrid frequency, *i.e.* $\omega = 10\omega_{LH}$. The electron cyclotron frequency is equal to $\omega_{ce} = 5.27\times10^6\ \mathrm{rad/s}$. The low frequency dipole antenna for excitation of ELF waves in the case of parametric excitation was driven by a current, $I_d = 2\ A$, oscillating at the frequency $\Omega = 8.54\times10^4\ \mathrm{rad/s}$. This frequency is well above the ion cyclotron frequency $\omega_{ci} = 2.64\times10^3\ \mathrm{rad/s}$ in the system. The table below gives several simulation parameters for the large 3D simulation performed for analysis of efficiency of whistler wave excitation.

Table 1: 3D PIC simulation Parameters

Simulation Time	$2.15e4\ ns$
Dipole Antenna Periods Simulated	3.49
Particles per cell	8
Total Particles	$5.64e9$
Processors	512
X, Y Size	$1680\ m$
Z Size	$1000\ m$
Computation Time	$\sim 3\ Weeks$

Two simulations were performed; one with a simple loop and one with a parametric antenna consisting of a loop and a dipole antenna. These simulations were otherwise identical. The resulting electric and magnetic field magnitudes were qualitatively and quantitatively very similar when considering all wavelengths. However, the differences are more apparent when k-space is filtered to separate the electromagnetic dominant wavelengths from the electrostatic dominant wavelengths. The isometric plots below show the electromagnetic part of the excited VLF wave spectrum.

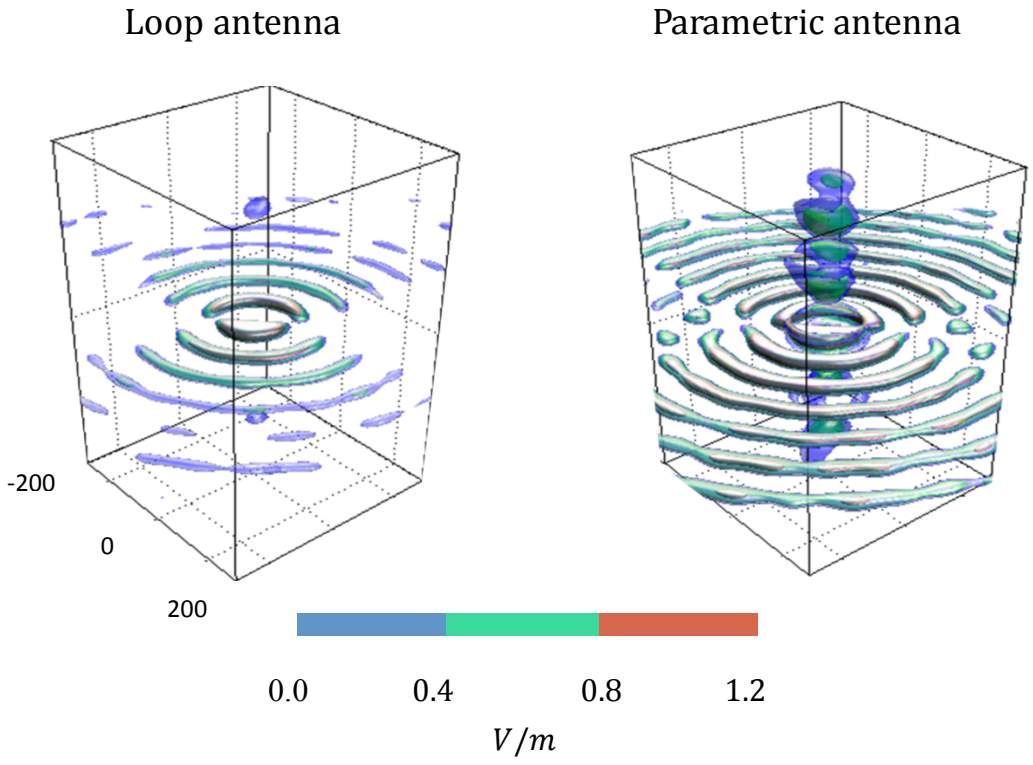

Figure 9: 3D Particle-In-Cell Simulation Results. Iso-surfaces of $E_{\perp}$ for $k < \frac{\omega_{pe}}{c}$, $B_o \parallel \hat{Z}$ Electromagnetic part of the excited wave spectrum of electric field: Excited by a loop antenna (left panel), Excited by a parametric antenna (right panel).

Using obtained simulation data we can calculate electromagnetic part of radiated power in the case of a single loop antenna as well as parametric antenna. To do so like in the previous sections, we can use (4) and (11). The simulation results for a single loop antenna with a loop plane perpendicular to an external magnetic field are as follows: for a single loop antenna for a long wavelength $\left(k_{\perp} < 0.25\frac{\omega_{pe}}{c}\right)$ electromagnetic part of the radiated power we found $P_L = 0.175\, Watts$ and for the power of parametrically excited whistler waves we have $P_{NL} = 2.313\, Watts$. This implies that for a given choice of initial plasma parameters and antenna currents the parametric antenna radiates approximately 13 times more power into the electromagnetic part of the VLF wave spectrum.

6. Nonlinear Interaction of VLF and ELF Waves at the TPBL

Broadband, oblique VLF whistler (W) waves at frequencies much greater than the lower hybrid resonance frequency have been detected in the TPBL, which is devoid of substorm-injected keV electrons (Mishin et al., 2011; Mishin, 2013). These emissions represent a distinctive subset of the substorm/storm-related VLF whistler activity and provide the rate of pitch-angle diffusion of the radiation belt electrons that can explain the plasmapause-RB boundary correlation (Mishin et al., 2011).
As the "standard" whistler generation mechanism by energetic electrons is unavailable in the TPBL, Mishin and Sotnikov (2017) suggested nonlinear interactions between quasi-electrostatic lower hybrid oblique resonance (LOR) and MS waves to be the source. Indeed, all three modes (ELF, LOR, and W) belong to the same branch with the cold-plasma dispersion relation (e.g., Sagdeev et al., 1977; Ganguli et al., 2010), known as Fast Magnetosonic Wave (FMS). In the case when $\omega_{pe} >> \omega_{ce}$ the eigen-frequency of FMS can be written as:

$$\omega_{\mathbf{k}}^2 = \frac{\omega_{LH}^2}{1+\frac{\omega_{pe}^2}{k^2c^2}}\left(1+\frac{M}{m}\frac{k_z^2}{k^2}\frac{1}{1+\frac{\omega_{pe}^2}{k^2c^2}}\right) \tag{20}$$

At different wavelengths and propagation angles ELF, LOR waves can easily couple with each other to produce a whistler wave.

Here $k^2 = k_{\|}^2 + k_{\perp}^2$, $k_{\|} = k_z = \mathbf{k}\cdot\mathbf{B}_0 / B_0$, $\mathbf{B}_0$ is the background magnetic field, ω_{ce} and ω_{pe} are the electron cyclotron and plasma frequencies, $\omega_{LH} = \sqrt{1+\frac{\omega_{pe}^2}{\omega_{ce}^2}} \approx \mu^{1/2}\omega_{ce}$ is the lower hybrid resonance frequency (at $\omega_{ce} \ll \omega_{pe}$), and $\mu = M/m$ is the ion-to-electron mass ratio.

In order to explain oblique VLF whistler waves at $\omega_w \geq 5\omega_{LH}$ observed in the TPBL (Mishin & Burke, 2005, Figure 3; Mishin et al., 2010, Figure 1; Mishin, 2013, Figures 4-5), Mishin & Sotnikov (2017) analytically explored parametric interaction of LOR waves at $\omega_1 = \omega_{\mathbf{k}_1} \gg \omega_{LH}$ with ELF waves at $\Omega_2 = \Omega_{\mathbf{k}_2} \ll \omega_{LH}$. This paper presents the results of numerical solution of a system of nonlinear equations describing parametric interactions between LOR and ELF pump waves excited in the TPBL by a hot ion-ring instability. Hot ion-ring provides LOR pump wave but does not affect nonlinear interaction. These simulation results show that nonlinear parametric interaction of the LOR and MS waves leads to oblique electromagnetic VLF (whistler) emissions at frequencies much greater than the lower hybrid resonance frequency, in agreement with the observations.

In general, parametric interaction of two waves, $\omega_{\mathbf{k}_1}$ and $\Omega_{\mathbf{k}_2}$, produces sidebands at the combination frequencies, $\omega_{\pm}$, that satisfy the matching conditions (e.g., Galeev and Sagdeev, 1979)

$$\omega_{\pm} = \omega_{\mathbf{k}_1} \pm \Omega_{\mathbf{k}_2} \text{ and } \mathbf{k}_{\pm} = \mathbf{k}_1 \pm \mathbf{k}_2$$

In the case in question, we have $\omega_{\pm} \sim \omega_{\mathbf{k}_1} \gg \Omega_{\mathbf{k}_2}$, i.e., the high-frequency (henceforth, VLF) and low-frequency (henceforth, ELF) counterparts, with $|\mathbf{k}_{\pm}| \ll |\mathbf{k}_1| \sim |\mathbf{k}_2|$. A general approach for solution of this problem was developed to explain symmetric sidebands, $\omega_{\pm}$, observed during active experiments with injection of a high-power VLF pump whistler wave (Sotnikov et al., 1991) and modulated electron beam (Sotnikov et al., 1994) into the ionosphere. It was shown that the beat waves of the VLF pump and natural ELF waves excite nonlinear currents that suffice to produce the observed VLF sidebands. That turns out to be just an initial step in the formation of a broadband VLF spectrum, because interaction of the sidebands with ELF produces secondary sidebands around the primary sidebands and so on. Thus, the relevant system of equations should be general enough to describe a broad range of wave numbers and frequencies. Sotnikov et al. (1991; 1994; 2018) and Mishin & Sotnikov (2017) used equations in the spectral, $(\omega, \mathbf{k})$, form, just enough for estimates of the sideband amplitude. In order to describe transition to the turbulent stage, equations in time-space coordinates are required. For this particular parametric process, hydrodynamic equations of motion for magnetized electrons and unmagnetized ions are used together with Maxwell's equations. The problem is essentially three-dimensional due to the so-called vector nonlinearity (e.g., Shapiro et al., 1993; Ganguli et al., 2010) and includes two systems of equations for ELF and VLF waves interconnected through nonlinear terms. As a result of combersome but

straightforward manipulations as Sotnikov et al.'s (1991; 1994; 2018), we get equations for the VLF and ELF potentials denoted as φ and Φ, respectively:

$$\partial_t^2(\Delta-\omega_{pe}^2/c^2)\Delta\left(\Delta+\frac{\omega_{pe}^2}{\omega_{ce}^2}(\Delta_\perp-\omega_{pe}^2/c^2)\right)\varphi+\left(\mu(\Delta-\omega_{pe}^2/c^2)+\nabla_z^2\right)\Delta^2\omega_{pe}^2\varphi=$$
$$=\frac{4\pi\omega_{pe}^2}{c^2\omega_{ce}}\partial_t^2(\Delta-\omega_{pe}^2/c^2)\left(en_0\left[\nabla,\mathbf{v}_{nl}\right]_z+\left[\nabla,\mathbf{j}_{nl}\right]_z\right)-4\pi e\partial_t(\Delta-\omega_{pe}^2/c^2)\Delta\nabla(\mathbf{V}\delta n_e+\mathbf{v}N_e)- \quad (21)$$
$$-\frac{4\pi\omega_{pe}^2}{c^2}\Delta\nabla_z(en_0\Psi_z-\partial_t\mathbf{e}_z\cdot\mathbf{j}_{nl})-4\pi en_0(\Delta-\omega_{pe}^2/c^2)\Delta\left(\partial_t\nabla_\perp\mathbf{v}_{nl}+\nabla_z\Psi_z\right)$$

$$\Delta\left\{\frac{\omega_{pe}^4}{\omega_{ce}^2c^4}\partial_t^2-\Delta\left(\frac{\mu\omega_{pe}^2}{c^2}-\nabla_z^2\right)\right\}\Phi=\frac{4\pi e}{c^2}\partial_t\Delta\nabla_\perp(\mathbf{v}^*\delta n_e+\mathbf{v}\delta n_e^*)+ \quad (22)$$
$$+4\pi\frac{\omega_{pe}^2}{\omega_{ce}c^4}\partial_t^2\left(en_0\left[\nabla,\mathbf{V}_{nl}\right]_z+\left[\nabla,\mathbf{J}_{nl}\right]_z\right)-4\pi en_0\partial_t\Delta\left(\nabla_\perp\mathbf{V}_{nl}\right)$$

Here we denote the VLF and ELF variables by the low-case and capital letters, respectively; $\partial_t=\partial/\partial t$, $\partial_t^2=\partial^2/\partial t^2$, $\left[\nabla,\mathbf{a}\right]_z=\left[\nabla\times\mathbf{a}\right]\cdot\mathbf{e}_z$, $\mathbf{e}_z=\mathbf{B}_0/B_0$, Δ is Laplacian**,** $\Delta_\perp=\Delta-\partial^2/\partial z^2$, $\nabla_\perp=\nabla-\mathbf{e}_z\partial/\partial z$. It is assumed that the plasma density perturbations δn_e and N_e are much smaller than the background density n_0. The r.h.s. of equations (21)-(22) include terms nonlinear in the wave amplitudes, such as nonlinear currents $\mathbf{j}_{nl}=-e\mathbf{v}\delta n_e$ and $\mathbf{J}_{nl}=-e(\mathbf{v}^*\delta n_e+\mathbf{v}\delta n_e^*)$, and nonlinearities due to the ponderomotive and Lorenz forces:

$$\Psi_z=(\mathbf{v}\nabla)V_z+(\mathbf{V}\nabla)v_z-\omega_{ce}\left(\left[\mathbf{v},\mathbf{B}/B_0\right]_z+\left[\mathbf{V},\mathbf{b}/B_0\right]_z\right) \quad (23)$$

The VLF (ELF) electron velocity $\mathbf{v}$ ($\mathbf{V}$), magnetic field $\mathbf{b}$ ($\mathbf{B}$), δn_e (N_e), and $\mathbf{v}_{nl}$ ($\mathbf{V}_{nl}$) are related to the potentials and each other via separate differential equations. Note that the cold, collisionless plasma approximation is used. In the following, length scales and wavelengths

perpendicular and parallel to $\mathbf{B}_0$ are normalized by $\lambda_e = c/\omega_{pe}$ and $\lambda_e \mu^{-1/2}$, respectively. The time, wave amplitudes, density perturbations, and perpendicular (parallel) velocities are normalized by the inverse VLF pump (LOR) angular frequency, ω_1^{-1} (dimensionless time $\hat{t} = \omega_1 \cdot t$), the VLF pump potential, φ_0, the background density, n_0, and $\omega_1 \lambda_e$ ($\omega_1 \lambda_e \mu^{-1/2}$), respectively. To numerically solve the resulting system of nonlinear equations and calculate the power of VLF electromagnetic emissions a FORTRAN code was developed. The code allows studying the evolution of the electromagnetic field and electron density disturbance generated by nonlinear interaction of the VLF and ELF waves employing the predictor-corrector quasi-spectral scheme. The details of the computation can be found in Sotnikov et al. (2018). The elliptic type equations are solved by spectral method using 3D Fast Fourier Transform approach. The computational box was chosen to include 16 VLF wavelengths in the x-direction, two ELF wavelengths in the **y**-direction, and one ELF (about four VLF) wavelengths in the z-direction. Periodic boundary conditions are applied in all directions with the grid size of 256x32x128**.**

We solve an initial value problem with VLF and ELF pump waves turn-on all the time. The adaptive time stepping was implemented with initial dimensionless time-step $\Delta\hat{t} = 2\pi \cdot 10^{-2}$ ($\Delta t \approx 10^{-5}$ s). The computation takes a few days on a standard PC.The input conditions are taken close to the observed values in the plasmasphere (Mishin et al., 2010, Figure 1): $B_0 = 0.003$ G, $n_0 = 10^2$ cm $^{-3}$, $\omega_{ce} \approx 5.3 \cdot 10^4$ s $^{-1}$, $\omega_{pe} \approx 5.6 \cdot 10^5$ s $^{-1}$, and $\omega_{LH} \sim 1.2 \times 10^3$ s $^{-1}$. The input VLF pump wave is a monochromatic quasi-electrostatic LOR at $\omega_1 \approx 5\omega_{LH}$**,** with 3D wavevector $\mathbf{k}_1 \frac{c}{\omega_{pe}}$ = (8, 0, 0.94 $\mu^{-1/2}$ **),** and the amplitude $E_1 = |k_1| \cdot \varphi_0 = 2$ mV/m**.** The input ELF wave is a monochromatic ELF wave with $\Omega_2 \approx 0.77\omega_{LH}$**,** $\mathbf{k}_2 \frac{c}{\omega_{pe}}$ = (0, 0.05, 0.13 $\mu^{-1/2}$**),** and $E_2 = |k_2| \cdot \Phi_0 \approx 2$ mV/m. The values of ω_1 and $\mathbf{k}_1$, as well as Ω_2 and $\mathbf{k}_2$, satisfy the dispersion equation (20). Note that the pump wave parameters are chosen specifically so that they are close to but not exactly satisfy the resonance conditions (eq. (match)) required to get the maximal efficiency of parametric interaction, as described by Sotnikov et al. (1991; 1994). However, in the resonance case, the collisionless system (21)-(22) crashes after only a few time steps because of singularities that cannot be avoided, unless collisional terms are included.

Figure 9 shows the VLF disturbance potential, $\delta\varphi = \varphi / \varphi_0 - 1$, in the middle of 3D grid as a function of time, with the initial value, $\delta\varphi(0)$, of zero. As one can see, the dimensionless amplitude increases up to $|\delta\varphi| \sim 0.3$ in a few VLF periods ($T_1 = 2\pi / \omega_1 \approx 10^{-3}$ s), and then saturates exhibiting strong modulation at about the ELF period ($T_2 = 2\pi / \omega_2$) until the end of the run. Simulation was ended after about $\approx$ 0.18 sec when the VLF disturbance started increasing uncontrollably, presumably because some of the emerging VLF sidebands have become resonant with the ELF waves.

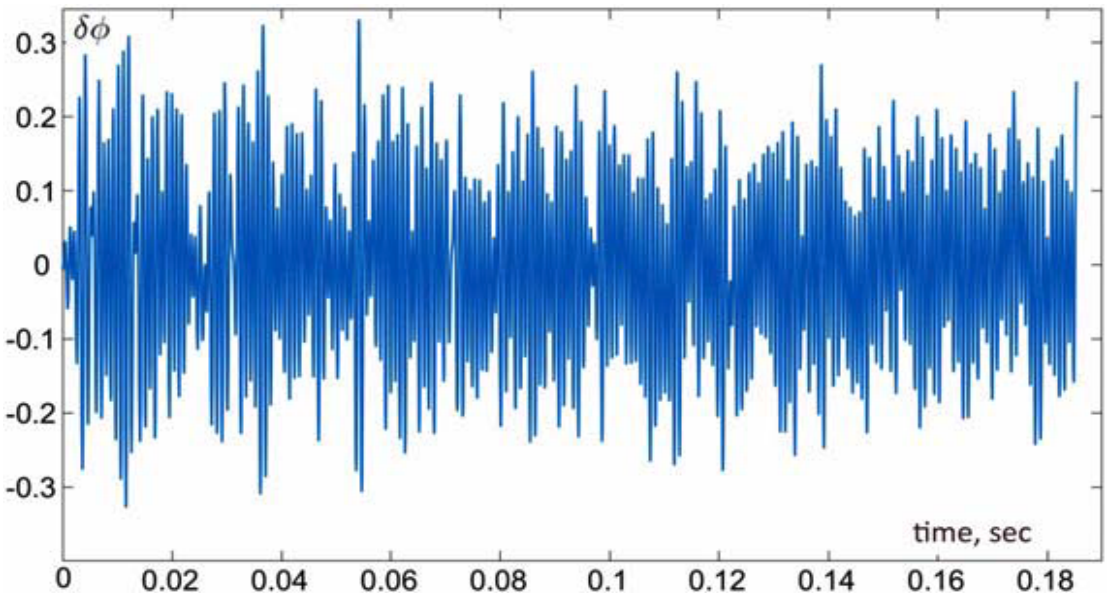

Figure 10. The VLF disturbance potential, $\delta\varphi$, generated by nonlinear interaction of VLF and ELF sources in the middle of 3D grid as a function of time. Note that the pump fields are not included in this and subsequent figures.

The spectral density of the VLF disturbance, $\delta\varphi$, near the end of the run (0.18 s) is shown in Figure 11. As anticipated, the spectrum includes two primary sidebands at $\omega_\pm = \omega_1 \pm \Omega_2$. Besides those, multiple secondary VLF sidebands of smaller amplitudes have emerged between 0.6 ω_1 and 1.4 ω_1 due to parametric interaction of the VLF sidebands with the ELF pump. Interactions of VLF sidebands with the VLF source and between each other result in the enhanced ELF disturbance, $\delta\Phi = \Phi / \Phi_0 - 1$.

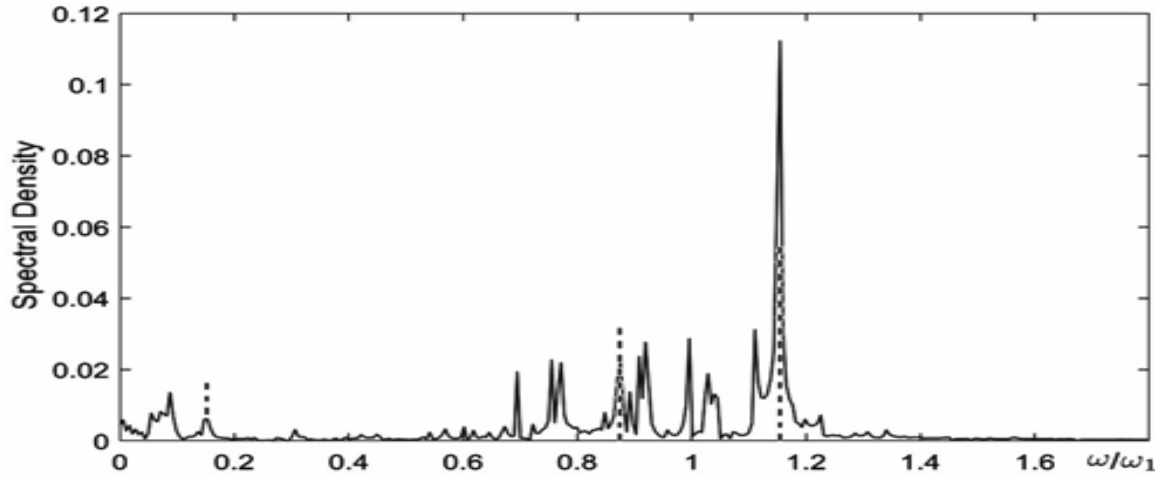

Figure 10. The spectral density of VLF waves in frequency domain in the middle of 3D grid at 0.18 s. The dotted lines show the frequencies of the ELF source and two primary sidebands.

Figure 11 shows two-dimensional spatial spectra of the VLF pump, φ_0 (frame a), and disturbance, $\delta\varphi$ (frames b, c, and d), taken at about 10^{-3}, 0.1, and 0.18 s in the middle of the computational domain at $y=16$, respectively. One can see that the spectral density of initially-absent large-scale modes inside the rectangles, placed in the region in k-space corresponding to electromagnetic whistler waves, increases with time due to cascading towards smaller wavenumbers. As a result, the final spectrum is enriched by large-scale electromagnetic VLF waves with k_z/k_x ranging from ~ 0.1 to ~ 0.6.

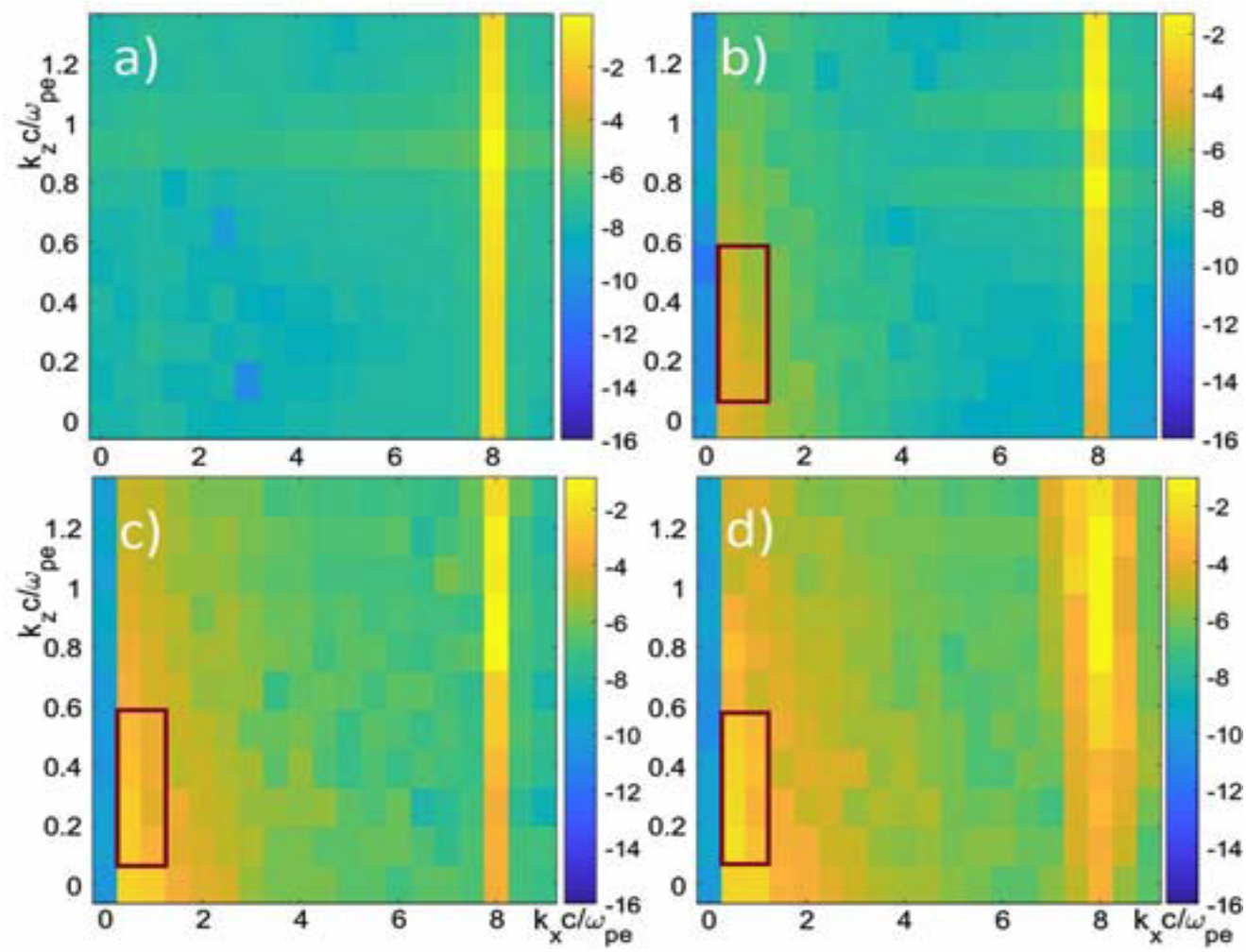

Figure 11. 2D Fourier spectra of the (a) VLF source and VLF disturbance at (b) one VLF period, (c) 96 VLF periods, and (d) 171 VLF periods. The wavenumbers inside rectangles correspond to the electromagnetic VLF emissions. Color codes in logarithmic scales are given to the right of the spectrograms.

The development of oblique VLF electromagnetic emissions with the wavenumbers inside the rectangles in Figure (3) 11 is further illustrated by Figure (4) 12, which shows the efficiency, $\kappa_W \approx \left(\frac{\omega_{ce}}{2\omega_w}\right)^{1/2} E_W / E_{LOR}$ (eq. (eff)), as a function of time. Here W_{LOR} is the total electrostatic VLF energy density outside the rectangles. The whistler wave amplitude increases with time up to the value of ~ 0.1 E_1 until the simulation is halted. This value is consistent with Mishin & Sotnikov's (2017) analytical **e**stimate and the observed VLF amplitudes.

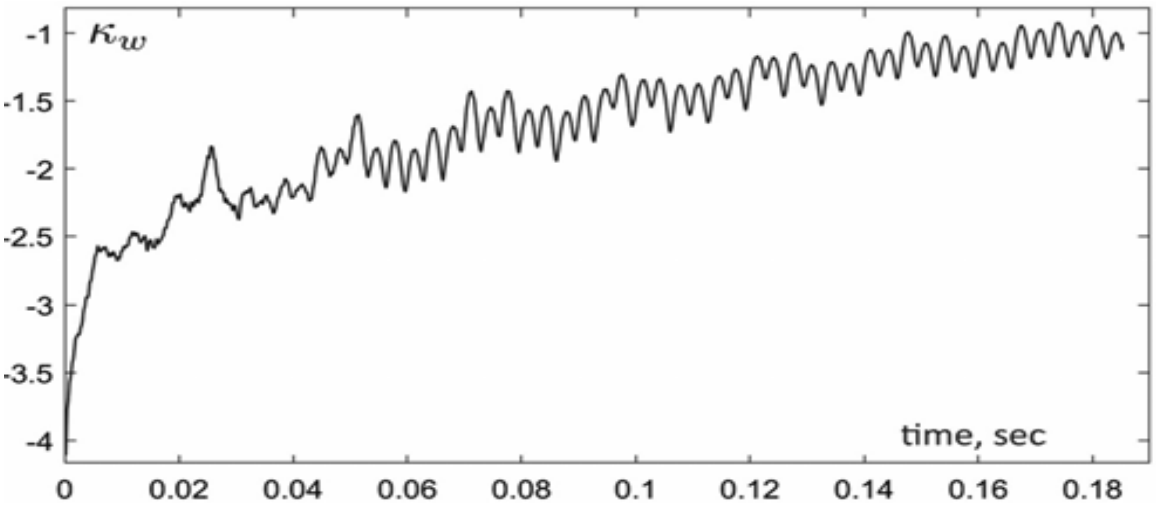

Figure 12. The VLF whistler generation efficiency $\kappa_w = \sqrt{W_w / W_{LOR}} \sim (\omega_{ce} / 2\omega_w)^{1/2} E_w / E_{LOR}$, in logarithmic scale vs. time.

The simulation results presented in Figures (1-4) 9-12 suggest the following scenario of parametric excitation of electromagnetic VLF (whistler) waves by the electrostatic VLF (LOR) and ELF pump waves. This process starts with the primary VLF sidebands, still close to the LOR branch, rapidly growing to large amplitudes of about 30% of the VLF pump amplitude. Since the parameters of the ELF pump and these sidebands are not synchronized for the resonance, the secondary sidebands have smaller amplitudes. As a result, it takes a considerable time, relative to the growth time of the primary sidebands, to create a broad spatial and temporal VLF spectrum (Figures (2) 10 and (3) 11). Therefore, the electromagnetic VLF disturbance, $\delta\varphi$, increases slowly with time. Note that the growing ELF disturbance, $\delta\Phi$ (not shown), practically does not influence the VLF emission. This conclusion follows from the comparison with the results of simulations with exactly the same input parameters but without taking account of the ELF disturbance.

A numerical model describing nonlinear parametric coupling of lower oblique resonance with fast magnetosonic waves in cold collisionless plasma has been developed in order to explain the generation of VLF electromagnetic (whistler) emissions in the turbulent plasmasphere boundary layer, which is devoid of energetic electrons. These emissions represent a distinctive subset of the substorm/storm-related VLF whistler activity interior to the plasma sheet inner boundary. The initial results of numerical simulations show that parametrically excited electromagnetic VLF emissions exhibit spectral features consistent with the observed VLF whistler waves. The presumed absence of dissipative processes has limited the applicability of the numerical model to about 180 VLF periods. Thereafter, some of the excited VLF

waves become resonant with the ELF pump resulting in the system's uncontrollable behavior due to singularities. Accounting for collisional damping is currently under way.

7. Conclusion

In this short review using analytical and numerical methods as well as PIC simulation we analyzed efficiency of excitation of electromagnetic whistler waves by a conventional loop antenna and by a combination of VLF loop and low frequency dipole antennas to excite whistler waves on combination frequencies.

It is worth mentioning that study of mode conversion between lower hybrid and whistler waves on short-scale density striations was carried out in [15].

Parametric interaction with two different low frequency modes was analyzed. In the case of parametric excitation first one was an ion acoustic mode (IA) and the second one was a fast magnetosonic (FM) mode. Results on parametric interaction of LOR waves excited by a loop antenna with ion acoustic (IA) waves and fast magnetosonic (FMS) waves demonstrate that this mechanism can be efficient enough to excite electromagnetic whistler waves with amplitude that can considerably exceed the amplitude of whistler waves directly excited by a loop. It was demonstrated that in the case of a single loop antenna only a small percentage of the radiated power ~ (3 – 5)% is going into an electromagnetic part of a VLF wave spectrum – a whistler mode. At the same time parametric mechanism of whistler wave excitation can provide much higher power radiated into an electromagnetic part of the spectrum. These results follow from both analytical solution in the case of interaction with IA waves and PIC simulation in the case of FM waves.

We have shown that whistlers in the spatial region between the resonance cone and the shadow boundary may be excited by the transformation of LOR waves excited by a high frequency antenna (ω ~ several ω_{LH}) on density perturbations generated by a low frequency source. Essentially, it amounts to a parametric excitation of whistlers in a volume of the plasma around the resonance cone. As the phase space volume for the nonlinear excitation is increased, the nonlinear whistler amplitude may be expected to be greater than the linear one. Physically this means that the volume of the parametrically excited plasma is substantially greater than the antenna itself.

Nonlinear coupling between VLF and IA waves as well as between VLF and ELF waves can give rise to sideband emissions. The amplitudes of the excited sidebands depend strongly on the frequency

mismatch $\delta\omega_{\pm} = \omega_{\mathbf{k}} \pm \Omega_{\mathbf{k}_s} - \omega_{\mathbf{k}\pm\mathbf{k}_s}$. It is possible to get values of $\delta\omega_{+}$: $\delta\omega_{-} << \Omega$ and values of the sideband amplitudes in agreement with experimental results. It is also possible to satisfy the condition for resonance excitation of VLF waves. If we take into account resonance broadening $\Delta\omega$ due to finite collisions then $\Delta\omega \sim \frac{\omega}{\omega_{ce}}\nu$, where ν is the collision frequency. This means that for nonresonant excitation of sidebands to occur $\delta\omega_{\pm} > \Delta\omega$ must be satisfied. In the opposite case when $\delta\omega_{\pm} < \Delta\omega$ resonant excitation mechanism takes place.

Acknowledgement

This work was supported by the Air Force Research Laboratory CRDF grant and Air Force Office of Scientific Research LRIR #19RVCOR038.

References

Bell T.F. and Wang T.N., (1971). Radiation resistance of a small filamentary loop antenna in a cold multicomponent magnetoplasma IEEE Trans. Antennas Propag. 517–22.

Bell T.F., H.G. James, H.G., Inan, U.S., Katsufrakis, J.P., (1983). The apparent spectral broadening of VLF transmitter signals during transionospheric propagation. J. Geophys. Res., 88, 4813 .

Bell T.F. and Ngo, H.D., (1988). Electrostatic waves stimulated by coherent VLF signals propagating in and near the inner radiation belt. J. Geophys. Res., 93, 2599.

Carpenter, D., and J. Lemaire (2004), The plasmasphere boundary layer, *Ann. Geophys*., *22,* 4291-4298.

Chmyrev V.M., (1989). Parametric excitation of ELF waves and acceleration of ions during the injection of strong VLF waves into ionospher, Kosm. Issled. 27, 249

Chugunov V., (1973). Electric characteristic of magnetic type exciters in plasma Sov. Izv. Vuzov Radiotechn. Electron. 18.6.

Eliasson, B., and K. Papadopoulos (2008), Numerical study of mode conversion between lower hybrid

and whistler waves on short-scale density striations, *J. Geophys. Res., 113*, A09315.

Inan U.S., and Bell, T.F., (1985). Spectral broadening of VLF transmitter signals observed on DE 1: A quasi-electrostatic phenomenon, J. Geophys. Res., 90, 1771.

Fiala V., Kruchina, E.N., Sotnikov, V.I., (1987). Whistler excitation by transformation of lower oblique resonance wave on density perturbations in the vicinity of a VLF antenna, Plasma Phys. Control. Fusion, 29, 1511.

Fisher R.K. and Gould R.W., (1971). Resonances cones in the field pattern of a radio frequency probe in a warm anisotropic plasma Phys. Fluids 857.

Foster, J., Erickson, P., Baker, D., Jaynes, A., Mishin, E., Fennel, J., Li, X., Henderson, M., & Kanekal, S. (2016). Observations of the impenetrable barrier, the plasmapause, and the VLF bubble during the 17 March 2015 storm. *J. Geophys. Res. Space Physics*, 121, 5537-5548.

Galeev, A., & Sagdeev, R. (1979). Nonlinear plasma theory, *in Reviews of Plasma Phys.*, v. 7, pp.1-180, Leontovich, M.A. (ed.), Consultants Bureau, New York.

Ganguli, G., L. Rudakov, W. Scales, J. Wang, and M. Mithaiwala (2010), Three dimensional character of whistler turbulence, *Phys. Plasmas, 17*, 052,310.

Goldstein, J., S. Kanekal, D. Baker, and B. Sandel (2005), Dynamic relationship between the outer radiation belt and the plasmapause during March--May 2001, *Geophys. Res. Lett., 32*, L15104.

Gringauz, K. (1983). Plasmasphere and its interaction with the ring current. *Space Sci. Rev.,* 34, 245-257.

Groves K.M., Lee, M.C., Kuo, S.P., (1988). Spectral broadening of VLF radio signals traversing the ionosphere J. Geophys. Res. 93, 14, 683.

Karpman V.I., (1986). Resonance cones of ring antennas in a magnetized plasma Sov. Fiz. Plasmy 12, 836.

Karpman V.I 1987 Electromagnetic field created by a dipole exciter in an anisotropic medium Phys. Lett. A 121 164.

Kondrat'ev I.G. and Kudrin A.V., (1992). Radiation of whistler waves in magnetoactive plasma Radio Sci. 27, 315–24.

Kudrin A.V., Petrov E.Y. and Zaboronkova T.M. (2001). Current distribution and input imipedance of a loop antenna in a cold magnetoplasma J. Electromagn. Waves Appl. 1569–3937.

LaBelle, J., & Treumann, R. (1988). Current-driven lower hybrid waves at the inner edge of the ring current. *J. Geophys. Res*., 93, 2591-2598.

Lagoutte D., Lefeuvre, F., Hanasz, J., (1989). Application of bicoherence analysis in study of wave interactions in space plasma. J. Geophys. Res. 94, 435.

Lee M.C. and Kuo, S.P., (1984). Production of lower hybrid waves and field-aligned plasma density striations by whistlers. J. Geophys. Res. 89, 10873.

Li, X., Baker, D., O'Brien, T., Xie, L., & Zong, Q. (2006). Correlation between the inner edge of outer radiation belt electrons and the innermost plasmapause location. *Geophys. Res. Lett.,* 33, L14107.

Mishin, E., & Burke, W. (2005). Stormtime coupling of the ring current, plasmasphere and topside ionosphere: Electromagnetic and plasma disturbances. *J. Geophys. Res.,* 110*,* A07209.

Mishin, E., Puhl-Quinn, P. A., & Santolik, O. (2010). SAID: A turbulent plasmaspheric boundary layer. *Geophys. Res. Lett.*, 37, L07106.

Mishin, E., Albert, J., & Santolik, O. (2011). SAID/SAPS-related VLF waves and the outer radiation belt boundary. *Geophys. Res. Lett.,* 38, L21101.

Mishin, E. (2013). Interaction of substorm injections with the subauroral geospace: 1. Multispacecraft observations of SAID. *J. Geophys. Res. Space Physics,* 118, 5782-5796.

Mishin, E., & Sotnikov, V. (2017). The turbulent plasmasphere boundary layer and the outer radiation belt boundary. *Plasma Phys. Control. Fusion,* 59, 124003.

Mishin, E., Nishimura, Y., & Foster, J. (2017). SAPS/SAID revisited: A causal relation to the substorm current wedge. *J. Geophys. Res. Space Physics,* 122, 8516-8535.

Mithaiwala, M., Rudakov, L., & Ganguli, G. (2010). Stability of an ion-ring distribution in a multi-ion component plasma. *Phys. Plasmas,* 17, 042113.

Mithaiwala, M., Rudakov, L., Ganguli G., & Crabtree, C. (2011). Weak turbulence theory of the nonlinear evolution of the ion ring distribution, *Phys. Plasmas,* 18, 055710.

Mishin, E.V., and Sotnikov, V.I., (2017). The turbulent plasmasphere boundary layer and the outer radiation belt boundary, Plasma Phys. Control. Fusion 59, 124003

Riggin, D. and Kelley, M.C. (1982). The possible production of lower hybrid parametric instabilities by VLF ground transmitters and by natural emissions. J. Geophys. Res. 87, 2545

Sagdeev R.Z., Sotnikov, V.I., Shapiro, V.D. and Shevchenko, V.I. (1977). To the theory of magnetosonic turbulence, JETP Letters, pp. Vol. 20,No 26,. 582.

Shapiro, V., Shevchenko, V., Solov'ev, G., Kalinin, V., Bingham, R., Sagdeev, R., Ashour-Abdalla, M., Dawson, J., & Su, J. (1993). Wave collapse at lower-hybrid resonance. *Phys. Fluids*, B, 5, 3148-3162.

Sotnikov V.I., Fiala, V., Lefeuvre, F., Lagoutte, D., and Mogilevsky, M., (1991). Excitation of sidebands due to nonlinear coupling between a VLF transmitter signal and a natural ELF emission, J. Geophys. Res.96, A7, 11363-2156-69.

Sotnikov V.I., Solovyev, G.I., and Fiala. V., (1993). Structure of the near zone electric field and the power radiated from a VLF antenna in the ionosphere Radio Sci. 28 1087.

Sotnikov V.I., Schriver, D., Ashour-Abdalla, M., and Ernstmeyer, J., (1994). Excitation of sideband emissions by a modulated electron beam during the CHARGE 2B Mission, J. Geophys. Res.99, A5, 8917.

Sotnikov V.I., Schriver, D., Ashour-Abdall, M., Ernstmeyer, J., and Myers, N., (1995). Excitation of electrostatic waves by a gyrating electron beam during the CHARGE-2B mission J. Geophys. Res. 100, 19765.

Sotnikov V., Kim, T., Caplinger, J., Main, D., Mishin, E.V., Gershenzon, N., Genoni, T., Paraschiv, I., and Rose, D., (2018). Parametric excitation of very low frequency (VLF) electromagnetic whistler waves and interaction with energetic electrons in radiation belt Plasma Phys. Control. Fusion 60, 044014

Sotnikov, V., Fiala, V., Lefeuvre, F., Lagoutte, D., & Mogilevsky, M. (1991). Excitation of sidebands due to nonlinear coupling between a VLF transmitter signal and a natural ELF emission, *J. Geophys. Res*., 96, 2156-2169.

Sotnikov, V., Schriver, D., Ashour-Abdalla, M., & Ernstmeyer, J. (1994). Excitation of sideband emissions by a modulated electron beam during the CHARGE 2B mission. *J. Geophys. Res.*, 99, 8927-8923.

Sotnikov, V., Ivanov, V., Presura, R., Leboeuf, J., Onishchenko, O., Oliver, B., Jones, B., Mehlhorn, T. & Deeney, C. (2008). Investigation of compressible eectromagnetic flute mode instability in finite beta plasma in support of Z-pinch and lLaboratory astrophysics experiments. *Comm. Comp.Physics*, 4, 611-623.

Sotnikov, V., Kim, T., Caplinger, J.,Main, D., Mishin, E., Gershenzon, N., Genoni, T., Paraschiv I., & Rose, D. (2018). Parametric excitation of very low frequency (VLF) electromagnetic whistler waves and interaction with energetic electrons in radiation belt. *Plasma Phys. Control. Fusion*, 60, 044014 (7pp).

Tanaka, Y., Lagoutte, D., Hayakawa, M., Tajima, M.S., (1987). Spectral broadening of VLF transmitter signals and sideband structure observed on Aureol 3 satellite at middle latitudes, J. Geophys. Res.,92,7551,1987.

Titova E.E., Di, V.I., Yurov, V.E., Raspopov, O.M., Trakhtengertz, V.Yu., Jiricek, T., Triska P., (1984). Interaction between VLF waves and the turbulent ionosphere. Geopys. Res. Lett, 11, 323.

Wang, T.N.C., and Bell, T.F., (1970). On VLF radiation resistance of an electric dipole in a cold magnetoplasma Radio Sci. 605.

Wang, T.N.C., (1974). On VLF input impedance of a loop antenna in a warm collisionless multicomponent magnetoplasma J. Geophys. Res. 79, 1073.

Wang, T.N.C., and Bell, T.F., (1969). Radiation resistance of a short dipole imersed in a cold magnetoionic medium Radio Sci. 167.

Wang,T.N.C., and Bell,T.F., (1972a). VLF/ELF radiation patterns of arbitrarily oriented electric and magnetic dipoles in a cold lossless multicomponent magnetoplasma J. Geophys. Res.,1174.

Wang, T.N.C., and Bell, T.F., (1972b). VLF/ELF input impedance of an arbitrarily oriented loop antenna in a cold collisionless multicomponent magnetoplasma IEEE Trans. Antennas Propag., 394.

Welch, D.R., Rose, D.V., Cueno, M.E., Campbell, M.R. and Mehlhorn, T.A., (2006). Integrated Simulation of the generation and transport of proton beams from laser-target interaction, Physics of Plasmas, 14.

Winske, D., & Daughton, D. (2012), Generation of lower hybrid and whistler waves by an ion velocity ring distribution. *Phys. Plasmas,* 19, 072109.

PA Approval #: 88ABW-2019-3589